Scanning Electron Microscopy

Volume 1982
Number 1 *1982*

Article 27

1982

Monte Carlo Simulation of Electron Scattering in Resist Film/ Substrate Targets

Kenji Murata
University of Osaka Prefecture

Electron Beam Interactions With Solids (Pp. 311-329)
SEM, Inc., AMF O'Hare (Chicago), IL 60666, U.S.A.

MONTE CARLO SIMULATION OF ELECTRON SCATTERING IN RESIST FILM/SUBSTRATE TARGETS

KENJI MURATA
Electronics Department, College of Engineering
University of Osaka Prefecture, 4-804 Mozu-umemachi
Sakai, Osaka 591, Japan
Phone: 0722-52-1161 Ext. 2286

ABSTRACT

First the fundamentals of resist modelling required to implement an analysis of developed resist patterns were studied, which represents the relationship between the energy deposited by incident electrons and the solubility characteristics of a positive or negative resist. Next, two models of single elastic scattering and fast secondary (knock-on) electron production were studied for Monte Carlo simulation of electron scattering in resist film/substrate targets, and the statistical errors of Monte Carlo results were evaluated. Finally, problems in electron beam lithography were investigated with the simulation. The exposure intensity distribution was studied with the two models. A comparison between Monte Carlo calculations and experiments shows that a better agreement is obtained with the knock-on model. An analysis of developed negative resist patterns has been performed by using Monte Carlo results for energy dissipation. A comparison with experimental results revealed that developed resist patterns deform while being stuck to the Si surface by a strong adhesion. Also the time evolution of developed profiles of PMMA (polymethyl methacrylate) resist films was investigated based on the Monte Carlo results for energy dissipation. A quantitative comparison between theory and experiment suggests that some modification is necessary for the empirical constants in the solubility rate due to the electron beam irradiation effect. The spatial resolution was examined for an isolated PMMA film. Resolutions of 320 Å and 530 Å were found with the single scattering and the knock-on models, respectively. The result with the knock-on model is similar to an experiment value of 600 Å obtained previously. It seems that the knock-on model may be useful for a theoretical study of the ultimate resolution in electron beam lithography.

Keywords: Monte Carlo simulation, electron scattering, fast secondary electrons, electron beam lithography, electron resists (polymethyl methacrylate, polyglycidyl methacrylate), resist modeling, exposure intensity distribution, proximity effect, backscattered electrons, statistical errors.

1. INTRODUCTION

Recent developments of semiconductor devices such as large scale integrated circuits owe much to very accurate fabrication technologies. One of these important technologies is electron beam lithography (EBL), which usually makes use of a finely focused electron beam in the same manner as in the scanning electron microscope. Spatial resolution of a few tens of nanometers with EBL has been achieved with a specific sample geometry consisting of thin PMMA (polymethyl methacrylate) resist films on thin substrates (Broers 1981). Fine pattern fabrication technologies will give a great impact on scientific or technological development in various fields if their advantages are put to good practical use. However, there is generally an obstacle in performing a high resolution due to electron scattering. This phenomenon is a very important factor, especially for the normal case of a resist film on a substrate such as that used in the semiconductor device fabrication. When incident beams depict a pattern on the resist film, electron scattering occurs in three different ways: (1) the forward scattering within the resist, (2) the backward scattering from the substrate, and (3) the backward scattering within the resist. These phenomena deteriorate the definition of depicted patterns by influencing other patterns nearby the electron incident position. This effect is called the proximity effect.

The present paper treats this kind of electron scattering problem in resist films with Monte Carlo simulation. Pattern fineness also depends on successive chemical development processes. Prior to going into details about simulation models, some fundamentals of resist modelling will be described. Two models are described about the Monte Carlo simulation: the single scattering model and the hybrid model (or the knock-on model) including fast secondary electron production which has been recently developed. Finally, applications of these simulations to EBL will be discussed, emphasizing electron-beam interactions with solids. As for an overall review on exposure and development models in EBL, the reader can refer to a recent review paper by Hawryluk (1981).

2. FUNDAMENTALS OF RESIST MODELLING

When energetic electrons are incident on electron resist films which are usually organic polymers with high molecular weight, these electrons collide with atoms or molecules com-

LIST OF SYMBOLS

G = Radiation yield (events/100eV).
$\bar{M}_n$ = The number average molecular weight before electron irradiation.
$\bar{M}_f$ = The number average molecular weight after electron irradiation.
D = Absorbed energy density (eV/cm³).
ϱ = Density (G/cm³).
N_A = Avogadro's number 6.02×10^{23} atoms/mole.
S = Solubility rate (A/sec).
R_0 = Constant in the solubility rate equation.
B = Constant in the solubility rate equation.
A = Constant in the solubility rate equation.
Δt = A short time to dissolve a resist cell with finite size.
Δd = Resist cell size.
n_R = Direction of etching in the ray tracing model.
S_{max} = The maximum value of the solubility rate S(X, Y) at position (X,Y).
p = Remaining film thickness d normalized by initial thickness d_0 of a negative resist film.
Q = Electron dose (C/cm²).
γ_r = Resist contrast.
dE/dz = Energy dissipation as a function of depth z (eV/cm).
$\bar{D}$ = Averaged absorbed energy density in a vertical parallel piped (eV/cm³).
$d\sigma_i^{el}/d\Omega$ = Differential elastic scattering cross-section of an atom i.
e = Electronic charge.
Z_i = Atomic number of an element i.
p = Electron momentum.
v = Electron velocity.
ω = Scattering angle.
β_i = The screening parameter for an atom i.
h = Planck's constant.
a_0 = Bohr radius.
σ_i^{el} = The total cross-section of an atom i.
$P(\omega)\, d\Omega$ = The probability that an electron is scattered into a small solid angle $d\Omega$.
ϕ = Azimuthal angle.
R = Uniform random number.
$F(\omega)$ = Integrated function of $P(\omega)\, d\Omega$.
n_i = The number of i atoms per unit volume.
C_i = Concentration of an element i.
P_i = The probability that an electron interacts with an atom i when collision occurred.
Λ_{el} = The mean free path for elastic scattering.
$p(\Delta s)$ = The probability that an electron travels the step length Δs between elastic scattering events.
dE/ds = Energy loss per increment of path length (eV/cm).
E = Electron energy.
J_i = The mean ionization potential (eV).
γ = Constant in the Bethe equation taking 2 or 1.166, depending on a non-relativistic or a relativistic electron, respectively.

LIST OF SYMBOLS

E_n = Electron energy at the n-th step in Monte Carlo simulation.
Δs_n = Step length of the n-th step in Monte Carlo simulation.
ϵ_c = Cut-off energy normalized by the initial energy E for energy transfer.
ϵ = Energy transfer normalized by the initial energy E_0.
m = Electron mass.
$[dE/ds]_{Single}$ = Energy loss due to secondary electron production.
$[dE/ds]_{Bethe}$ = Continuous energy loss rate.
$d\sigma/d\epsilon$ = Differential inelastic cross-section (cm²/eV).
$[d\sigma/d\epsilon]_M$ = Differential inelastic cross-section of Moller.
τ = Kinetic energy normalized by the rest mass energy.
σ^{in} = The total cross-section for inelastic scattering.
Λ_{in} = The mean free path for inelastic scattering.
Λ_{tot} = The mean free path for elastic and inelastic scattering.
σ_{tot} = The total cross-section for elastic and inelastic scattering.
p^{el} = The probability that an electron suffers an elastic scattering when a collision occurred.
p^{in} = The probability that an electron suffers an inelastic scattering when a collision occurred.
$P_m(s)$ = The probability that electrons travel a distance s in the m-th layer without being scattered after one scattering event.
W_m = The total cross-section in the m-th layer.
a_m = The maximum depth in the m-th layer.
n_{im} = The number of i atoms per unit volume in the m-th layer.
σ_{im}^{el} = The total elastic cross-section of an i atom in m-th layer.
Λ_m = The mean free path for elastic scattering in the m-th layer.
Λ_{PMMA} = The mean free path for elastic scattering in the PMMA layer.
Λ_{Si} = The mean free path for elastic scattering in the Si layer.
n = The number of backscattered electrons.
η = The backscattering coefficient.
N = The number of incident electrons.
η_N = The backscattering ratio at N trials of the event.
D_c = The critical absorbed energy density.
$f(r)$ = Exposure intensity distribution as a function of radial distance r.
$F(E)$ = The total absorbed energy in a resist film.
η_E = Ratio of the energy deposited by backscattered electrons to that by forward scattered electrons.
β_f = Spreading width by forward scattered electrons.
β_b = Spreading width by backward scattered electrons.
T = Development time.

posing the polymer, and excite or ionize them through inelastic scattering events, resulting in chemical changes in the polymeric state. This change occurs in two different ways, i.e., molecular chain scission which causes the degradation of molecular weight and cross-linking which causes gel formation in the polymer. Generally these processes occur in the same resist. Types of positive or negative resist behaviour are determined by which process is dominant. In this section a brief description of modelling for both resists is given, separating these types.

2.1 Modelling for positive resist

(A) Degradation of molecular weight and solubility rate changes. The change of mean molecular weight due to electron beam exposure can be evaluated (Ku and Scala 1969, Herzog et al. 1972), without going into detailed processes of ionization and excitation of molecules or atoms, by introducing a radiation yield G which is defined as the number of bonding or scission events caused by an energy absorption of 100 eV from incident electrons. Assume the molecular weight distributions before and after electron irradiation are shown in Fig. 1, which have the number average molecular weights $\bar{M}_n$ and $\bar{M}_f$, respectively. If the absorbed energy density is D at an arbitrary location in the resist, then the number of scission events is GD/100 in the unit volume. This must be equal to the difference between the initial number of molecules $(\varrho/\bar{M}_n)N_A$ and the final number of molecules $(\varrho/\bar{M}_f)N_A$, where ϱ is the mass density of the resist and N_A is Avogadro's number. This relation is written in the following form:

$$\bar{M}_f = \left(\frac{1}{\bar{M}_n} + K\right)^{-1}$$

$$\text{or} \quad \frac{\bar{M}_f}{\bar{M}_n} = \frac{1}{1+\bar{M}_n K} \qquad 1$$

where $K = GD/100\,\varrho N_A$.

The above equation means that in order to obtain the same value of the degradation ratio $\bar{M}_f/\bar{M}_n$, the amount of dose D can be decreased, if the value of $\bar{M}_n$ is increased. If we can find the fractional molecular weight $\bar{M}_f$, then the empirical formula for the solubility rate can be established with a certain solvent. This is expressed by the following equation (Greeneich 1974, 1975).

$$S = R_0 + B \cdot \bar{M}_f^{-A} \qquad 2$$

The constants R_0, B and A are determined experimentally. A typical value of A is approximately 1 to 4, depending on the developer. The larger the value of A, the weaker the developer.

(B) Etching model. Developed resist profiles of electron exposed regions depend on development time as well as a solvent, development temperature, etc. The kind of profile has an important meaning in a microfabrication process such as the lift-off technique.

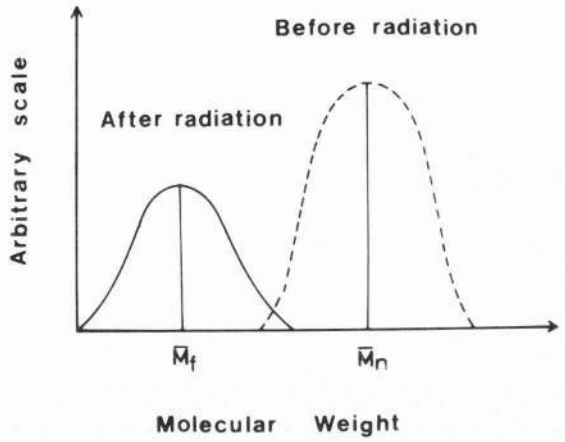

Fig. 1. The molecular weight distributions for positive electron resist before and after electron irradiation.

With the solubility rate of a resist as mentioned before, it is possible to simulate the time evolution of developed profiles if the spatial distribution of the absorbed energy density is found in a resist film. The following three models have been proposed for this purpose (Jewett et al. 1977).

(i) Cell model
(ii) String model
(iii) Ray tracing model

The cell model is applied to two dimensional profiles such as the case of a long line exposure. A resist film is divided into small cells. A time to dissolve cells exposed to the solvent is calculated successively as follows by using Eq. 2.

$\Delta t = \Delta d/S$ when one face is exposed to a developer
$\Delta t = \Delta d/\sqrt{2}\,S$ when two adjacent faces are exposed

where d is the cell size. The total time to reach the cell (i,j) is obtained by summing up sequential development times. This method is easy to organize with a computer program for calculation. Recently a new calculation has been proposed for a three dimensional analysis (Jones et al. 1981).

The string model forms a string combined with representative points in the resist. These points advance step by step during a short period Δt at the solubility rate which is calculated from the absorbed energy density. The direction of motion is determined by a bisector of the angle made by the two adjacent strings.

The ray tracing model is based on an analogy to Snell's law for light ray refraction. The ray traces the direction of a vector $n_R = S_{max}/S\,(X,Y)$ where S_{max} is the maximum value of the solubility rate, S(X,Y). The line connected with the end of the ray gives an etched profile.

The latter two models, which can be easily extended to the three dimensional calculation, are expected to give a better accuracy than the first one, but the computer programming will be somewhat harder. If we simulate the etched profiles of a resist pattern with a weak developer by using the resist etching model above, we find that a weak developer has a high contrast. That means it responds sensitively to a change of the fractional molecular weight of the resist or the absorbed energy density. Namely, a front surface of etch pro-

file does not move further when it meets an appropriate slope in the energy absorption distribution. Then the etched profile is along the equi-energy density contour. This is called the critical absorbed energy density model or the threshold model (Herzog et al. 1972, Greeneich and Van Duzer 1974).

2.2 Modelling for negative resist

Different from positive resist, a negative resist remains insoluble in the exposed region due to gel formation caused by cross-links among neighbouring molecules, depending on exposure dose. The insoluble fraction of the resist is related to the gel fraction, which determines the remaining film thickness $p = d/d_0$, normalized by initial thickness (Atoda and Kawakatsu 1976). Usually the relation between the dose Q and the remaining thickness p is given by the so-called contrast curve. A typical example of experimental data is shown in Fig. 2 for a 6000 Å PGMA (polyglycidyl methacrylate) resist film at 10 keV. The cure time is 30 min. The developer is a solution of 7 MIBK (methyl isobutyl ketone) and 1 EtOH (ethanol). The development temperature is 22-23°C. The rinse was done with MIBK for 30 sec. No post baking is done. A straight line portion of the curve can be given by the following equation:

$$P = \gamma_r \log_{10} (Q/Q_m) \qquad 3$$

where γ_r is the resist contrast ($\gamma_r = 1.12$ in the figure), and Q_m the minimum dose at which thickness remaining is observed. Heidenreich et al. (1975) and Lin (1975) have performed a developed profile analysis of negative resist based on these contrast curves. They assumed a Gaussian distribution for a line exposure dose. Although they gave an expression to take account of the lateral spreading of an electron beam, the effect is neglected in the actual calculation. Nakata et al. (1981) tried to analyze a pattern of lines and spaces by using the spatial distribution of the absorbed energy density which is obtained by Monte Carlo calculation. The calculation procedure is described briefly. The depth distribution of the absorbed energy density is not uniform as seen from Fig. 3, which was obtained by Monte Carlo calculation for the same conditions as that in Fig. 2. For simplification a uniform depth distribution is assumed as shown by a dotted line in Fig. 3. Then, we can replace the dose Q (C/cm^2) on the abcissa by the absorbed energy density D(eV/cm^3) which is obtained by the product of $[dE/dz]_{AV}$ ($eV/C \cdot cm$) and Q (C/cm^2). The theory that the gel fraction is associated with the absorbed energy density has been developed based on the radiation yield G (Charlesby 1954, Atoda and Kawakatsu 1976). In the figure a dotted line shows the theoretical curve calculated by the Charlesby theory, assuming both the Schultz-Jim function for the molecular weight distribution of polymer and the inhibitor activity i, using the average absorbed energy in Fig. 3.

As shown in Fig. 4, the resist film is divided into many vertical parallel-pipeds. In each pipe the absorbed energy density is averaged over depths, and then from the contrast curve the gel fraction, i.e., the normalized remained film thickness is found, corresponding to the averaged energy density $\bar{D}$. This process throughout all pipeds makes up the developed patterns.

3. MONTE CARLO SIMULATION OF ELECTRON SCATTERING IN ELECTRON RESISTS

The first Monte Carlo simulation of electron scattering was reported by Green (1963) in the fields of electron probe microanalysis (EPMA) and scanning electron microscopy (SEM). This simulation utilized experimental data for the angular distribution of electron scattering. With this simulation it was suggested that the Monte Carlo technique is useful for prediction and explanation of electron scattering phenomena in EPMA and SEM targets. In 1965 the Multiple Scattering Monte Carlo model was successfully applied to the calculation of X-ray production by Bishop (1966), Shimizu et al. (1966) and Shinoda et al. (1968) based on Lewis' multiple scattering theory, which was used for high energy electrons (Berger 1963). In 1968 Reimer published the single scattering model based on the Rutherford cross section for elastic scattering and the Bethe law for energy loss. Subsequent work on the single scattering model has been reported by Reimer et al. (1970), Curgenven and Duncumb (1971), McDonald et al. (1971), Murata et al. (1971). The models used are somewhat different from each other. After this, many investigations on electron scattering in EPMA and SEM targets were published with these models. Based on these past studies the Monte Carlo simulation with the single scattering model was applied to fundamentals of electron beam lithography. The reports by Shimizu and Everhart (1972) and Shimizu et al. (1975) were concerned with energy dissipation in bulk PMMA targets. The reports by Saitou (1973), Hawryluk et al. (1974) and Kyser and Murata (1974) handled energy dissipation in thin films on substrates. These reports have promoted applications of the calculations to the practice of electron beam lithography as mentioned in the latter section. The multiple scattering model is not useful for a lithography application because the mean free path for scattering is too long compared to resist film thickness. The hybrid model with single and multiple scattering regions might be useful for the present application, which was proposed by Newbury et al. (1980). Adesida et al. (1979) and Adesida and Everhart (1980) applied the direct Monte Carlo simulation which was developed by Shimizu et al. (1976). This new model is powerful to accurately predict the energy distribution of transmitted electrons through a thin film.

Recently Monte Carlo calculations have been performed including the effect of fast secondary electron production with a hybrid model for the discrete and continuous energy loss process (Murata et al. 1981). Two typical models of the single scattering model and the hybrid model are described here:

3.1 Single Scattering model

Incident electrons which penetrate a specimen undergo their direction of motion and energy losses through elastic and inelastic scattering events with atoms, respectively. Some electrons are backscattered through large angle-single scattering or small angle-multiple scattering and escape from the specimen. Some penetrate deep depths and lose all energy within the specimen. This complicated electron trajectory can be simplified by separating the effects of elastic and inelastic scattering events. Namely, the angular deflection is determined by the elastic scattering and the energy loss be-

tween scatterings is calculated by the continuous slowing-down approximation of the Bethe law. If the cross-section can be found for elastic scattering, the scattering mean free path Λ can be calculated between elastic collisions in a similar way to the theory for classical particles in a gas chamber, where the crystalline structure of the specimen can be neglected in the first approximation, that is, atoms are assumed to be distributed uniformly. The result is shown in Fig. 5. Three elements required in the simulation are given in the following:

(A) The distribution of scattering angles

We can simply use the following screened Rutherford equation for elastic scattering cross section:

$$\frac{d\sigma_i^{el}}{d\Omega} = \frac{e^4 Z_i^2}{p^2 v^2 (1 - \cos\omega + 2\beta_i)^2} \qquad 4$$

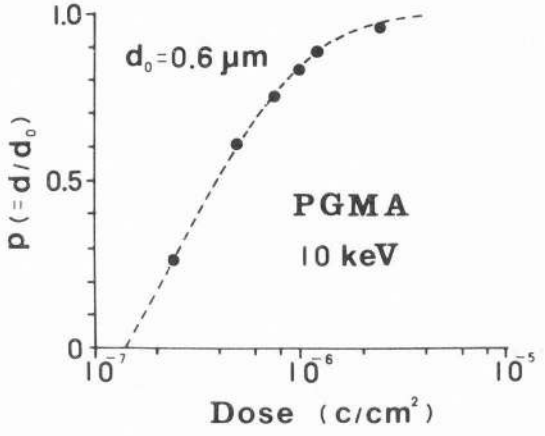

Fig. 2. The normalized remaining film thickness as a function of dose for negative electron resist PGMA.

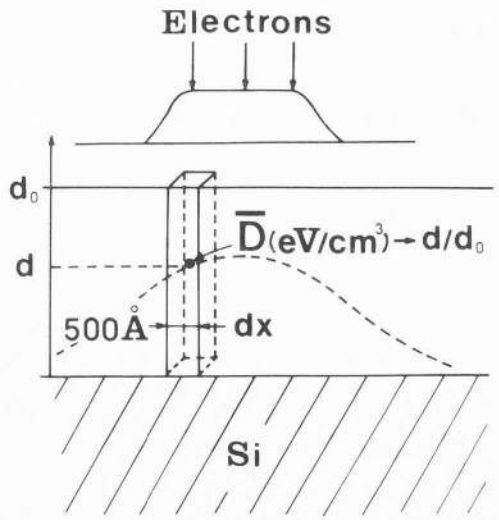

Fig. 4. The determination of the remaining film thickness with the averaged absorbed energy density within vertical parallelpipeds the cross-section of which is typically a (500 Å)^2 square.

where p is the electron momentum, v the velocity, e the electronic charge, Z_i the atomic number of an element i and β_i the screening parameter.

We can take account of the angular deflection due to electron-electron inelastic scattering simply by replacing Z_i^2 with $Z_i(Z_i + 1)$ assuming the Rutherford equation for the electron-electron coulomb scattering as well (Kulchitsky and Latyshev 1942). The following value of β_i is useful, which was obtained by Nigam et al. (1959) through use of the Thomas-Fermi type potential for electrostatic screening of the nucleus by the orbital electrons:

$$\beta_i = \frac{1}{4}\left(1.12\,\frac{h\lambda i}{2\pi p}\right)^2 \qquad 5$$

where $\lambda_i = Z_i^{1/3}/0.885a_0$, a_0: Bohr radius, h: Planck's constant.

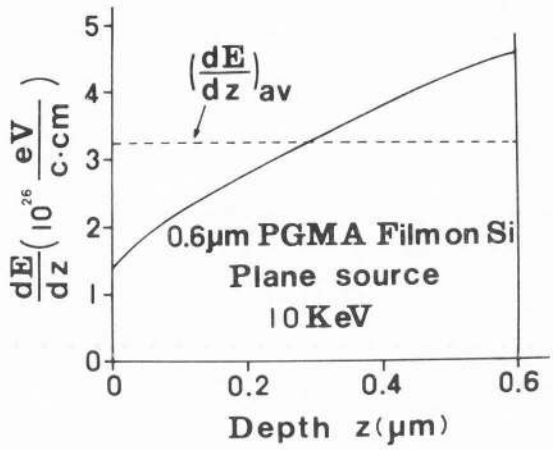

Fig. 3. The depth variation of absorbed energy in a 6000 Å thin negative resist at 10 keV obtained by Monte Carlo calculation. The average absorbed energy density was determined to be $(dE/dz)_{AV} = 3.24 \times 10^{26}$ eV/C·cm from this result.

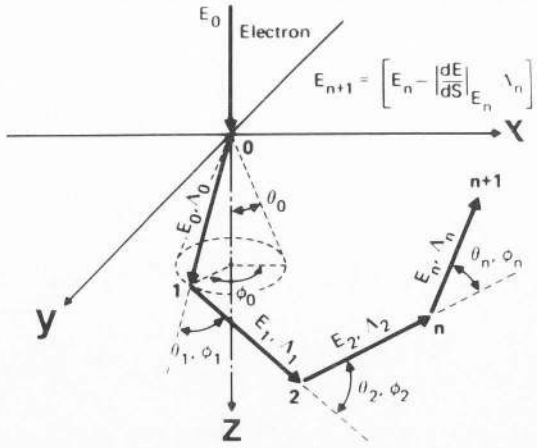

Fig. 5. Simplified electron trajectory for the single scattering model.

The total cross section of one atom can be calculated by integrating Eq. 4 as follows:

$$\sigma_i^{el} = \frac{\pi e^4 Z_i^2}{\beta_i(1+\beta_i)\, p^2v^2} \qquad 6$$

When one scattering event has occurred, the electron is scattered into a small solid angle $d\Omega$ with the probaility $P(\omega)$ as given by

$$P(\omega)\, d\Omega = \left(\frac{d\sigma_i^{el}/d\Omega}{\sigma_i^{el}}\right) d\Omega \qquad 7$$

By integrating this equation to an arbitrary value of ω, the probabilistic determination is made through use of a generated uniform random number R (hereafter R means a pseudo-uniform random number between 0 and 1 generated with a computer algorithm). Namely, a value of $\cos\omega$ can be decided by substituting R into $F(\omega)$ as follows:

$$\cos\omega = 1 - \frac{2\beta_i F(\omega)}{1+\beta_i - F(\omega)} \qquad 8$$

The analytical expression of Eq. 8 makes it easy to calculate the scattering angle.

The angle ϕ is assumed to be uniformly distributed around the axis of the electron travelling direction, and is determined by another uniform random number R, i.e., $\phi = 2\pi R$. When an electron travels the distance equal to the mean free path, one elastic collision always occurs. Then, which atom the electron collided with has to be determined. The sum of the total cross-section in a unit volume of a mixed element specimen can be calculated as follows:

$$\Sigma\, n_i \cdot \sigma_i^{el} = \Sigma \frac{C_i \varrho N_A}{A_i} \sigma_i^{el} \qquad 9$$

where C_i is the weight percent of an i-th element, ϱ the density, A_i the atomic weight and N_A Avogadro's number. Therefore, the probability for an i-th element scattering is given below:

$$P_i = \frac{n_i\, \sigma_i^{el}}{\Sigma\, n_i \sigma_i^{el}} = \frac{\dfrac{C_i \varrho N_A \sigma_i^{el}}{A_i}}{\Sigma \dfrac{C_i \varrho N_A}{A_i} \sigma_i^{el}} \qquad 10$$

where random numbers are alloted according to the probability P_i:

$$0 < R \le P_1,\ P_1 < R \le P_1 + P_2,$$
$$P_1 + P_2 < R \le P_1 + P_2 + P_3, \ldots \qquad 11$$

The collision atom is decided by which unequal equation a generated uniform random number falls between.

(B) Step length

The mean free path Λ_{el} for elastic scattering is the following:

$$(\Lambda_{el} = (\Sigma_i n_i \sigma_i^{el})^{-1} \qquad 12$$

If we adopt the mean free path as a step length, the procedure above mentioned for angular scattering can be utilized.

Variable step lengths can be used, which are distributed around Λ_{el} as follows:

$$P(\Delta S) = \frac{1}{\Lambda_{el}} \exp\left(-\frac{\Delta S}{\Lambda_{el}}\right) \qquad 13$$

In this case another uniform random number R or R′ is used to determine Δs in a similar way to the determination of the scattering angle ω.

$$\Delta S = -\Lambda_{el} \cdot \ell n\, \{1-R\} \equiv -\Lambda_{el} \cdot \ell n R' \qquad 14$$

(C) Energy loss

The continuous energy loss law of Bethe is used

$$-\frac{dE}{dS} = \frac{7.85\times10^4}{E} \varrho \Sigma_i \frac{C_i Z_i}{A_i} \ell n \frac{\gamma E}{J_i} \qquad 15$$

$$N_i = \varrho C_i N_A / A_i$$

where J_i is the mean ionization potential, and $J_i = 9.76Z_i + 58.5Z_i^{-0.19}$ has been often used (Berger and Seltzer 1964). The value of γ is 2 or 1.166 depending on a non-relativistic or a relativistic electron, respectively. The energy at the next step is simply calculated by the following:

$$E_{n+1} = E_n - \left|\frac{dE}{dS}\right|_{E=En} \cdot \Delta S_n \qquad 16$$

A shortcoming of the Bethe law at low energies is overcome by the following equation of Rao Sahib and Wittry (1974):

$$-\frac{dE}{dS} = \frac{7.85\times10^4}{1.26\sqrt{E}} \varrho \Sigma \frac{C_i \cdot Z_i}{A_i \sqrt{J_i}} \qquad 17$$

where $E \le 6.338\ J_i$. Similarly the equation developed by Love et al. (1977) can be used.

According to Spencer and Fano (1954), the Bethe law which has been derived for an infinite target has to be modified as shown in Eq. 18 when the boundary condition is taken into consideration that electrons are incident on the surface of a semi-infinite target:

$$\frac{dS}{dE} = -(KM)^{-1}\left(1 - \frac{\pi^2}{6} M^{-2}\right) \qquad 18$$

$$K = \frac{\pi e^4 \varrho N_A}{AE}$$

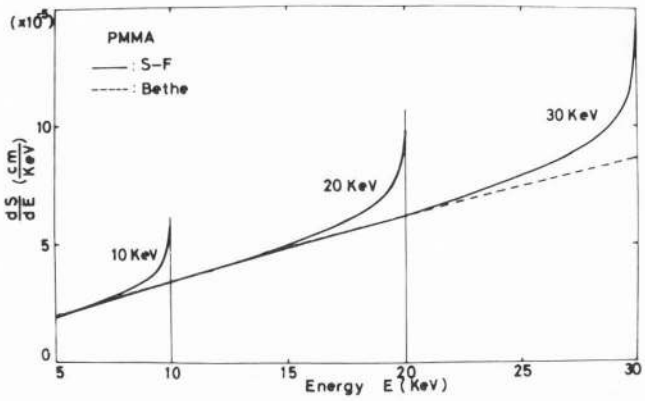

Fig. 6. A comparison in the reciprocal stopping power for PMMA at 10, 20 and 30 keV between the theories of Spencer-Fano and Bethe.

$$M = 1 + \ell n\{4E(E_0 - E) / J^2\} - \ell n\,(E_0/E)$$

This theory is based on the physical mechanism that discrete processes with a long mean free path for inelastic scattering have to be subtracted from all existing processes for electrons right after incidence on the target. The theory has no relativistic correction. Brown et al. (1969) first applied this correction to microanalysis with the EPMA, by using the following artifice for a relativistic correction:

$$ds/dE = [\text{non-relativistic expression of Eq. 15} \,/\, \text{relativistic expression of Eq. 15}] \times \text{Eq. 18.} \quad 19$$

This theory has been also utilized in a study of secondary electron emission by Shimizu (1974). Results of numerical calculations with Eq. 19 are shown in Fig. 6 for a target of PMMA at energies of 10, 20 and 30 keV.

3.2 Hybrid model for the discrete and continuous energy loss processes

The Bethe law (Eq. 15) is obtained by averaging various discrete energy losses which include the production of fast secondary electrons. From the Bethe range an electron with an energy of, say, 2 keV, can travel a distance of 1400 Å, neglecting a direction change due to inelastic collisions. These secondaries may cause spreading of energy absorption in addition to that with the old model as described in a previous section. An attempt in lithography applications has been published by Murata et al. (1981) based on the hybrid model for the discrete and continuous energy loss processes, which had been proposed originally by Schneider and Cormack (1959) and had been developed to a more theoretical treatment by Berger (1963, 1971) and Seltzer (1974).

(A) Energy loss. The energy loss process is shown schematically in Fig. 7. The dashed line shows the previous Bethe equation. From this continuous energy loss some discrete processes are picked up. Then the remaining energy loss resulting from a collection of small energy losses will form still a continuous component. This will be described for a non-relativistic electron by the following equation:

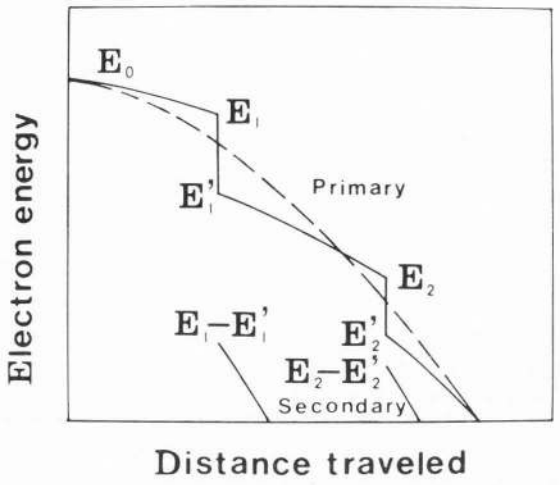

Fig. 7. Schematic illustration of an energy loss process in the hybrid model. Fast secondary electrons are generated at catastrophic collisions.

$$\left[\frac{dE}{dS}\right]_{\epsilon c} = \left[\frac{dE}{dS}\right]_{\text{Bethe}} - \left[\frac{dE}{dS}\right]_{\text{single}} \quad 20$$

where

$$\left[\frac{dE}{dS}\right]_{\text{single}} = \Sigma ni Zi \int_{\epsilon_c}^{1/2} E \cdot \epsilon \left[\frac{d\sigma}{d\epsilon}\right] d\epsilon \quad 21$$

where a cut-off value, ϵ_c, normalized by the initial energy E for energy transfer is introduced, and ϵ is the energy transfer normalized by the initial energy E. Collisions with energy transfer ϵ larger than ϵ_c is picked up among various energy loss processes. Knock-on electrons are generated through this process. The differential inelastic cross section $[d\sigma/dE]$ is an important quantity to determine the probability of fast secondary electron production. As there is no accurate theory for this cross-section, the following Moller equation for free electrons has been used, which gave the lowest cross section among the theories available at the moment:

$$\left[\frac{d\sigma}{d\epsilon}\right]_M = \frac{B}{E}\left\{\frac{1}{\epsilon^2} + \frac{1}{(1-\epsilon)^2} + \left(\frac{\tau}{\tau+1}\right)^2 - \frac{2\tau+1}{(\tau+1)^2} \cdot \frac{1}{\epsilon(1-\epsilon)}\right\} \quad 22$$

$$B = 2\pi e^4 / mv^2$$

where τ is the kinetic energy normalized by the rest mass energy of the electron. For small values of τ the equation reduces to the following:

$$\left[\frac{d\sigma}{d\epsilon}\right]_M = \frac{B}{E}\left\{\frac{1}{\epsilon^2} + \frac{1}{(1-\epsilon)^2} - \frac{1}{\epsilon(1-\epsilon)}\right\} \quad 23$$

Finally it follows that an electron loses energy continuously according to $[dE/ds]_{\epsilon_c}$ and it suffers a catastrophic energy change occasionally according to the knock-on cross section $[d\sigma/d\epsilon]_M$. The knock-on event is not continued for secondary electrons.

The cross section for inelastic scattering is calculated by

$$\sigma^{in} = \frac{\pi e^4}{E^2}\left\{\frac{1}{\epsilon_c} - \frac{1}{1-\epsilon_c} - \ell n\left(\frac{1-\epsilon c}{\epsilon_c}\right)\right\} \qquad 24$$

Because the Moller model is based on the free electron theory, there is no discrimination among electrons of any atom or any element.

(B) The distribution of scattering angles. For elastic scattering the same equation as used in the single scattering model is adopted for both primary and secondary electrons. In this model Z^2 has not to be replaced by $Z(Z+1)$ as a correction for inelastic scattering because this is accounted for by Eqs. 25 and 26 for primary and secondary electrons, respectively,

$$\sin^2\theta = \frac{2\epsilon}{2+\tau-\tau\epsilon} \qquad 25$$

$$\sin^2\phi = \frac{2(1-\epsilon)}{2+\tau\epsilon} \qquad 26$$

These equations will be the following when $\tau \ll 1$, which gives a classical binary collision of nonrelativistic electrons:

$$\sin\theta = \sqrt{\epsilon} \qquad 27$$

$$\sin\phi = \sqrt{1-\epsilon} \qquad 28$$

(C) Step length. In the present model two probabilistic events, i.e., elastic and inelastic scattering are considered in the determination of the mean free path. Therefore, the mean free path Λ_{tot} is given by the harmonic mean as follows:

$$\Lambda_{tot}^{-1} = \{\Sigma n_i \cdot \sigma_i^{el} + \Sigma n_i Z_i \sigma^{in}\} = \sigma_{tot} \qquad 29$$

$$= \Lambda_{el}^{-1} + \Lambda_{in}^{-1}$$

The variable step length is calculated with a uniform random number R:

$$\Delta S = -\Lambda_{tot} \cdot \ell n\, R \qquad 30$$

(D) Selection of elastic or inelastic scattering. The type of collision is determined by the probability of elastic (p^{el}) or inelastic (p^{in}) collision through use of a uniform random number R.

$$p^{el} = \frac{\Sigma n_i \sigma_i^{el}}{\sigma_{tot}} \qquad 31$$

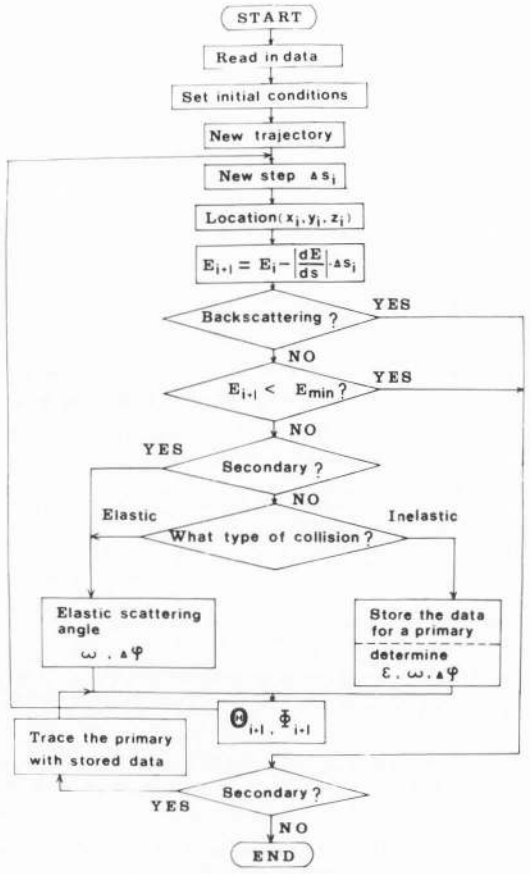

Fig. 8. Flow chart of the Monte Carlo calculation with the hybrid model.

$$p^{in} = \frac{\Sigma n_i Z_i \sigma^{in}}{\sigma_{tot}}$$

Finally, the new model is summarized in the following:

For Primary electron

(i) Energy loss: Moller equation / Modified Bethe equation

(ii) Angular deflection: Screened Rutherford eq. (elastic) / Moller theory (inelastic)

For Secondary electron

(i) Energy loss: Bethe equation

(ii) Angular deflection: Screened Rutherford eq. (elastic)

The flow chart of the calculation for the trajectory is briefly shown in Fig. 8. The program is made so as to perform the simulation with the new or the old model by putting an input data of $0 < \epsilon_c < 0.5$ or $\epsilon_c = 0.5$, respectively.

3.3 Simulation of electron scattering in resist films on substrates

The Monte Carlo simulation can handle any boundary condition easily such as the incident angle and the specimen geometry. In lithography applications a special specimen structure of a coated resist film on a substrate is required for the calculation. There are various possibilities of the location

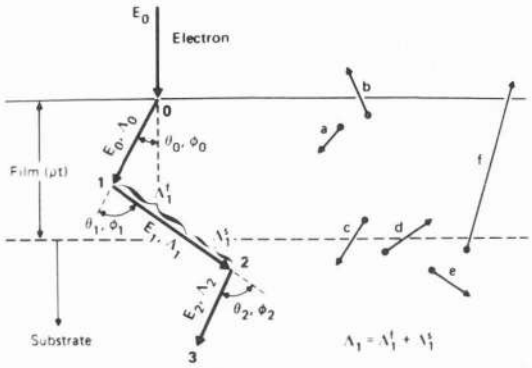

Fig. 9. Electron trajectory modelling for a sample of a thin resist film on a substrate.

of the step as shown in Fig. 9. This is shown in the right side of the figure. One problem occurs when the step crosses the interface of a resist-substrate. The first approximation is to use the step length which was determined at the initial position even when it crosses the interface (Kyser and Murata 1974). However, when the initial position comes close to the interface, the accuracy of this approximation becomes worse. Or in the case that there is a large difference between the mean free paths on both sides, larger errors are induced. Recently a new model to improve this deficiency has been published by Horiguchi et al. (1981). They introduced the differential equation for the probability $P_m(s)$ that electrons travel a distance $z=s$ in the m-th layer without being scattered after one scattering event.

$$dP_m(S) = - W_m P_m(S)\, dS \qquad 32$$

where $P_1(S=0) = 1$, $P_{m+1}(S=a_m) = P_m(S=a_m)$, and a_m is the maximum depth in the m-th layer, W_m is the total cross section in the m-th layer, which is given by

$$W_m = \Sigma\, n_{im} \cdot \sigma_{im}^{el} = \Lambda_m^{-1} \qquad 33$$

The solution of Eq. 32 gives the following probability $P_m(S)$ for the distribution of the variable step length:

$$P_m(S) = \frac{1}{\Lambda_1} \exp\left(-\frac{S}{\Lambda_1}\right), \text{ for } 0 \le S \le a$$

$$= \frac{1}{\Lambda_m} \exp\left[-\sum_{k=2}^{m} \left(\frac{1}{\Lambda_{k-1}} - \frac{1}{\Lambda_k}\right) a_{k-1} \right. \qquad 34$$

$$\left. - \frac{1}{\Lambda_m} \cdot S\right], \text{ for } a_{m-1} < S \ll a_m \; (m = 2,3,\ldots n)$$

$$= 0, \text{ for } a_m < S$$

In the usual manner the accumulated function F(s) of $P_m(s)$ is used to determine the variable length s.

According to the new model the mean free path Λ depends

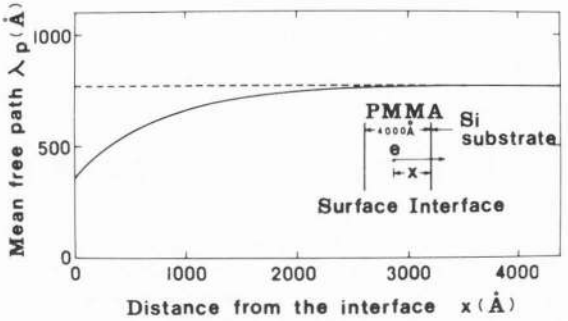

Fig. 10. The mean free path calculated with a new treatment at the boundary by Horiguchi et al. (1981). The result is shown for a 4000 Å PMMA film on a Si substrate at 20 keV. The old model assumes the constant mean free path as shown by the dashed line.

on the initial position of an electron. Let us take an example of a 4000 Å PMMA resist film on a Si substrate. Λ can be calculated as follows for an electron at a distance x from the interface:

$$\Lambda = \int_0^X SP_1(s)dS + \int_X^\infty SP_2(s)dS \qquad 35$$

$$= \Lambda_{PMMA} - (\Lambda_{PMMA} - \Lambda_{Si}) \exp\left(-\frac{X}{L_{PMMA}}\right)$$

This equation reduces to

$$\Lambda = \Lambda_{Si}, \text{ for } X = 0 \qquad 36$$

$$= \Lambda_{PMMA}, \text{ for } X = \infty$$

The calculated result is shown in Fig. 10 at 20 keV. Horiguchi et al. (1981) have shown that the new model predicts very well experimental data of the backscattering intensity from the sample with the three layer structure of CMS (chloromethylated polystyrene) resist-Mo (0.3 μm)-Si. In the present paper this new model is not included.

3.4 The accuracy of the simulation

Generally, it is not easy to deduce the accuracy of Monte Carlo results. Statistical errors can be calculated by $\sqrt{n}$ for results such as the number, n, of backscattered electrons. Accordingly, the fluctuation of the backscattering coefficient η is given by

$$\pm \Delta\eta = \pm \sqrt{\frac{\eta}{N}}$$

where N is the number of incident electrons. According to the central limit theorem, the confidence interval of the probability p for occurrence of backscattering is given by the following (Miyatake and Nakayama 1963):

$$P_r\left(\frac{\eta_N + \frac{a^2}{2N} - \sqrt{D}}{1 + \frac{a^2}{N}} \le P \le \frac{\eta_N + \frac{a^2}{2N} + \sqrt{D}}{1 + \frac{a^2}{N}}\right)$$

$$\fallingdotseq \frac{2}{\sqrt{2\pi}} \int_0^a e^{-\chi^2/2} d\chi \qquad 37$$

where η_N is the backscattering ratio at N trials of the event,

$$D = (\eta_N + \frac{a^2}{2N})^2 - \eta_N (1 + \frac{a^2}{N}) \qquad 38$$

The inequality equation gives the confidence intervals of 95% and 99% for a=2 and 3, respectively. An example is shown in Fig. 11 for the backscattering from a thin resist film of 500 Å on an Si substrate. In the figure the confidence intervals are given for both 95% and 99%. The reliability increases rapidly around a few hundreds of incident electrons. This is supported from the fact that the statistical error, $\Delta\eta/\eta = (N\eta)^{-1/2}$, decreases from 27% to 8% for a change from 100 to 1000 incident electrons. The value of η becomes stable as the number of incident electrons increases. It will be difficult to apply the central limit theorem to the general case. For example although the energy absorbed in the thin resist per unit volume at a certain position is related to the number of electrons passing through that volume, the energy deposited is different, depending on electron energy. Some weighting factor has to be introduced in applying the theorem to a confidence interval estimate. Detailed discussions are not made further in the present paper. Only the variation of the Monte Carlo results is shown with the number of incident electrons.

To obtain the spatial distribution of energy dissipation, the Monte Carlo computer program divides resist space into concentric donut-shaped volumes for the case of a point source electron beam and into parallelpipeds for the case of a line source. Therefore, the accuracy of the calculation depends on the size of a small volume, the cross-section of which is usually taken to be square. The smaller the size, the higher the spatial resolution. But then the statistical error increases. In the present paper the size of the volume is usually 500 Å × 500 Å. But in case of need some plan has to be made that a smaller volume is used at either a position where higher resolution is required or at the higher intensity region, and a larger volume is used at a position where a lower resolution is sufficient owing to a gentle variation of the distribution. At least the statistical error can be decreased by taking advantage of the symmetry of co-axial or bi-axial geometries. Fig. 12 shows a typical result of the energy dissipation distribution in a resist film of 500 Å thickness on a Si substrate, which was calculated with the old model. The result is shown for representative points in the resist. Only 44, 36 and 10 electrons come into the 500 × 500 (Å²) volume at lateral distances of 0.05, 1.05 and 2.05μm, respectively, for 8900 incident electrons even though electrons are added due to bi-axial symmetry around the incident direction. It is found from the figure that in order to obtain a relatively stable result, incident electrons of a few thousand are required at a high intensity region, but more electrons are required at a low intensity region with the same spatial resolution.

Typical computational times with an IBM 370/168 computer for the case of a 4000 Å PMMA film on a Si substrate are 12 min and 37 min with the single scattering model and the knock-on model, respectively.

4. APPLICATION TO THE PRACTICE OF ELECTRON BEAM LITHOGRAPHY

The Monte Carlo simulation has been applied to various problems of electron scattering in EBL. Some papers are concerned with the fundamentals such as energy dissipation in a thick or thin resist film. Some are concerned with the cross sectional profile simulation of developed resist patterns. Some others study the proximity effect including its dependence on various experimental factors such as resist thickness, voltage, substrate, developer, etc. A detailed description of these investigations is beyond the scope of the present paper. Some typical fundamental problems which are not clear will be discussed, emphasizing electron beam interactions with solids.

4.1 Exposure Intensity Distribution

The spatial distribution of energy dissipation in a resist film on a substrate is called the Exposure Intensity Distribution (EID), which is generated by incidence of a finely focused electron beam. The distribution has a characteristic feature consisting of two parts: a sharp peak around the origin and a broad, low intensity background. The distribution has been investigated by many authors experimentally and theoretically because it is required in order to implement a proximity effect correction. The Monte Carlo simulation can easily generate this distribution as a function of radius. Experimentally it is obtained by dot exposures with a finely focused beam on a positive resist (PMMA) film on a substrate where dose has been changed over a wide range. After development of the exposed dots, the diameters of the removed area are measured with a scanning electron microscope. An appropriate value of the critical absorbed energy density has to be assumed in order to convert the experimental dose to the absorbed energy density. This kind of experiment has been carried out by Hawryluk et al. (1975), Adesida et al. (1979) and Murata et al. (1980). However, it will be difficult to measure a very small diameter when the dose is small. Therefore, usually the energy dissipation distribution as a function of lateral distance, which is obtained from line scan exposures, is shown as an EID curve instead of the radial distribution. The lateral distribution can be converted into the radial distribution by means of an Abel inversion assuming that the exposure effects are additive (Hawryluk et al. 1975). In Fig. 13 some results are compared between experiments of Hawryluk et al. (1975) and Monte Carlo simulations for a 4000 Å thick PMMA film on an Si substrate at 20 keV, assuming a value of 1.1×10^{22} eV/cm³ for Dc as reported by Hawryluk et al. (1975). Two theoretical results are shown in the figure with the new and the old models. Although the calculated results have a depth variation, they are compared at a depth of 1000 Å below the top of the resist surface according to the definition of the experimental line width by Greeneich and Van Duzer (1974). This is because the narrowest width observed from the experimental developed cross section by Wolf et al. (1971) exists inside, not at the surface which is predicted by theories of either analytical methods or Monte Carlo calculations. They assumed that possible reasons for the above discrepancy are the resist shrinkage at the surface and the electron current distribution. As pointed out by previous authors (Hawryluk et al. 1974, Adesida et al. 1979) the old model, i.e., the single

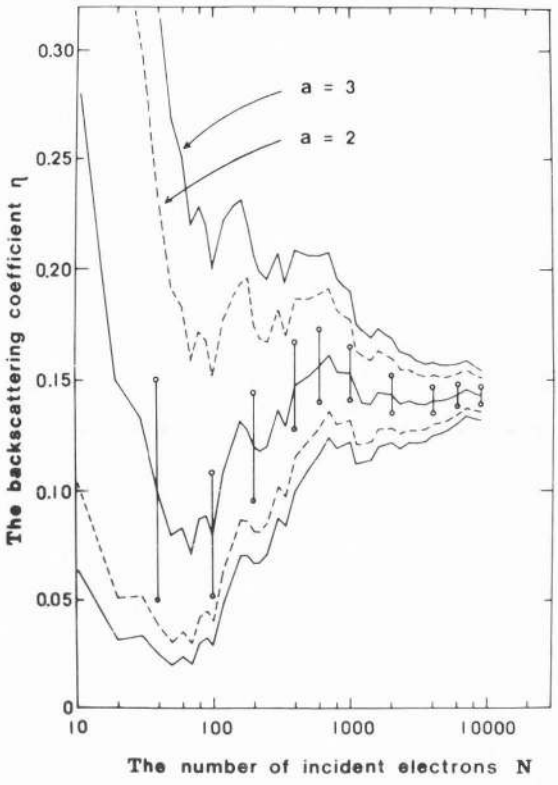

Fig. 11. A variation of the backscattering coefficient η with the number of incident electrons. The result is shown for a 500 Å PMMA film on an Si substrate at 20 keV. The figure includes a variation of the standard deviation (vertical lines with circles at both ends) and the confidence intervals of 95% (a = 2) and 99% (a = 3).

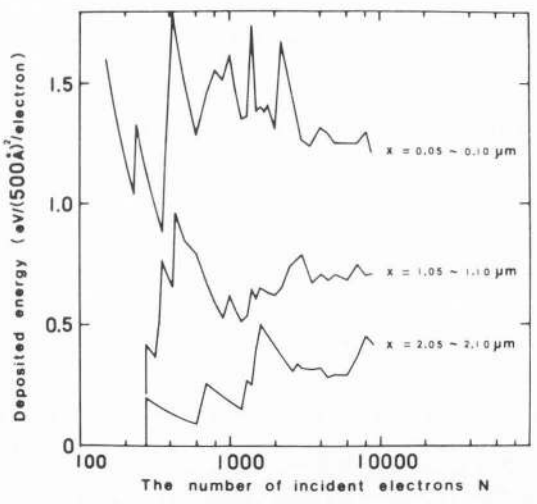

Fig. 12. A variation of the absorbed energy density with the number of incident electrons, which was obtained from the same calculation as in Fig. 11. Because of bi-axial symmetry the intensities for parallelpipeds with the same values of |x| are added together to enhance the statistical accuracy.

scattering model has a clear discrepancy near the incident position of an electron beam. This discrepancy is improved very much with the hybrid model, i.e., the knock-on model. A larger spreading near the origin is accounted for by the knock-on model which includes the effects of the energy straggling and fast secondary electron production. Another discrepancy is found at the tail. This is partly responsible for a low statistical accuracy as shown in Fig. 12.

Adesida et al. (1979) and Adesida and Everhart (1980) have done a similar experiment for various thicknesses of an Si substrate. They obtained $D_c = 1.5 \times 10^{22}$ eV/cm³ which is the same as in the present comparison. However, their Monte Carlo results with discrete processes included seem to have a little higher energy dissipation for the background intensity. Neglecting this difference, good agreement with experiments is obtained except for a discrepancy at the sharp peak which was found in the study by Hawryluk et al. (1975) as well. Their experimental data was examined with the Hybrid model of the simulation. First the critical absorbed energy density D_c was determined so that the Monte Carlo results of the absorbed energy density distribution fit approximately the experimental one for a thick substrate at 20 keV. The result is shown in Fig. 14. A large discrepancy is still found in the peak region. A value of D_c obtained is 4.4×10^{21} eV/cm³. By using the same value of D_c a comparison was made between theory and experiment for a 1000 Å PMMA film on a thin Si substrate (600 Å). This is shown in Fig. 15. We can see a relatively good agreement. This comparison is very im-

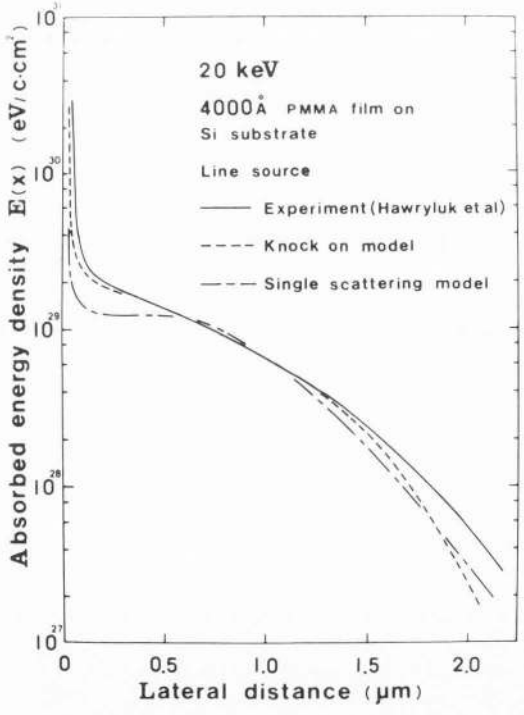

Fig. 13. The lateral distribution of the absorbed energy density for a 4000 Å PMMA film on an Si substrate at 20 keV. A comparison is made between the experimental data (Hawryluk et al. 1975) and the calculated results with two models.

portant to see how accurately the knock-on model can evaluate the resolution limit in the case that backscattering can be neglected.

As seen in Fig. 13, the EID curve is Gaussian like. Chang (1975) proposed an analytical expression with two Gaussian distributions based on his experimental data. This is given usually in the following form:

$$f(r) = \frac{F(E)}{\pi(1+\eta_E)} \left\{ \frac{1}{\beta_f^2} \exp\left(-\frac{r^2}{\beta_f^2}\right) + \frac{\eta_E}{\beta_b^2} \exp\left(-\frac{r^2}{\beta_b^2}\right) \right\} \quad 39$$

where β_f is the spreading width by the forward scattered electrons, β_b is the one by the backscattered electrons, and η_E represents the ratio of the energy deposited by the backscattered electrons to that by the forward scattered electrons. In Eq. 39 the depth variation is neglected. An integration of Eq. 39 over the whole area results in F(E). Consequently, F(E) is the total absorbed energy. As this expression is very convenient to calculate the energy absorption for an arbitrary pattern exposure which is required for a proximity effect correction, the parameters of β_f, β_b and η_E have been investigated by many authors. As these parameters depend upon many experimental factors such as resist thickness, developer, development conditions, initial accelerating voltage etc., it is difficult to establish a consistent theory to obtain them. A value for β_b is relatively easy to obtain because it has a large enough value to observe experimentally. Although β_f is not easy to estimate since its value is very small, it is not important practically because generally the beam size is dominant compared to the size of β_f except for the case of a thicker resist film, say larger than 1 μm. This will be important in the fabrication of a very fine pattern. The value of η_E is an important factor to determine the strength of background intensities in the proximity effect. Although many studies are conducted on η_E as summarized by Hawryluk (1961), it has a variety of 0.5-1.1. Although a qualitative dependence of η_E on the resist thickness, beam voltage and substrate materials is known, its quantitative understanding is not sufficient at the moment. The Monte Carlo result of η_E, which is obtained by the energy absorption, shows a lower value than the experimental one. As pointed out by several authors, this difference probably comes from the solubility characteristics of a solvent in the experiment. It has been shown by an indirect method of Kyser et al. (1980) that the Monte Carlo results combined with the solubility characteristics agree fairly well with the experimental values of η_E. This problem

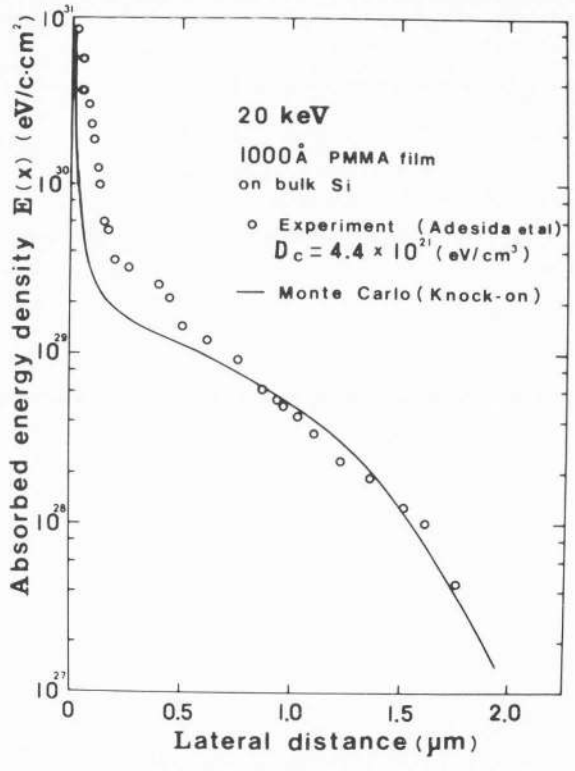

Fig. 14. The lateral distribution of the absorbed energy density for a 1000 Å PMMA film on an Si substrate at 20 keV are compared between experiment (Adesida et al. 1979) and Monte Carlo calculation with the knock-on model. A value of 4.4×10^{21} eV/cm³ is assumed for the critical absorbed energy density.

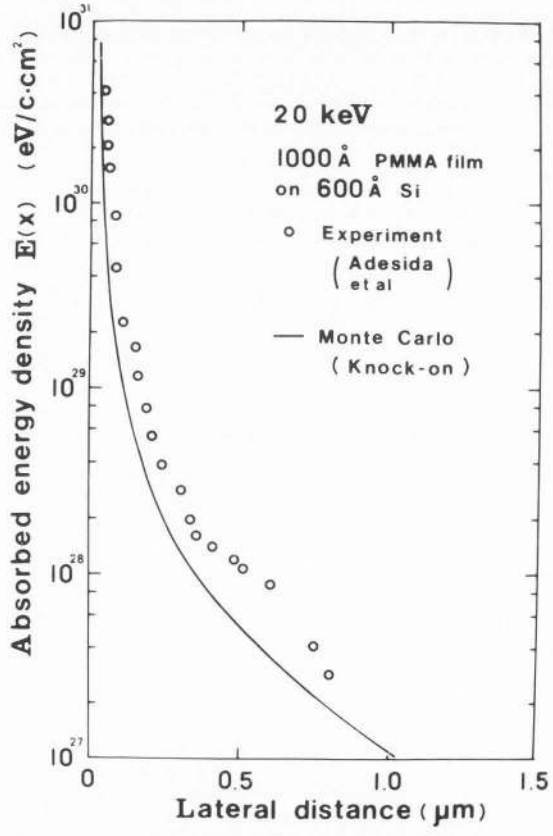

Fig. 15. The lateral distribution of absorbed energy for a 1000 Å PMMA film on a 600 Å thin Si substrate at 20 keV. The results are compared between experiment (Adesida et al. 1979) and Monte Carlo calculation with the knock-on model.

requires some more detailed discussions in the future. The reduction in the energy dissipation predicted by the theory of Spencer and Fano (1954) or the knock-on model may have to be included in further studies.

Analytical methods have been also developed to calculate the spatial distribution of dissipation energy. A detailed comparison between analytic methods and Monte Carlo calculations has been reported by Hawryluk et al. (1974, 1975, 1981). Generally the Monte Carlo method is expected to give a more accurate result in the cases of various resist thicknesses or/and initial energies and is more flexible to set various boundary conditions and specimen geometries. However, the Monte Carlo method has a great disadvantage in that much computational time is needed to obtain sufficient accuracy.

4.2 Negative resist pattern analysis

An analysis of negative resist patterns is troublesome because the resist shrinks and swells after development as clarified by the analysis based on the contrast curve by Heidenreich et al. (1975) and Lin (1975). Further study has been done by Nakata et al. (1981) using the Monte Carlo results for energy absorption. The experiment was performed under the same condition as when the contrast curve of Fig. 2 was obtained with the negative resist of PGMA exposed by a 10 keV electron beam of 2500 Å beam size with the EBMG-40 system. The patterns of equal lines and spaces of 1, 2 and 3 μm was exposed with 4, 8 and 12 single lines, respectively. After the development procedure above mentioned, cross-sectional profiles of the cleaved sample were observed with the scanning electron microscope. The results are shown in Fig. 16 for line and space patterns of 1 and 3 μm at a dose of 4.0×10^{-7} C/cm^2. Only the half part is shown due to symmetry. The top figure shows the equi-energy density contours calculated by the Monte Carlo simulation with the single scattering model taking into consideration the Spencer-Fano theory. The contours spread laterally near the pattern edge due to the proximity effect (in this case the intra-proximity effect). The effect appears as a gradual slope of the calculated profiles at the edge shown by a dashed curve. Experimental profiles shown by a solid line are different largely from the calculated results, which are unfavorable in the practical fabrication processing. This discrepancy suggests the hypothesis that the resist pattern shrinks laterally and swells longitudinally while being stuck at the interface due to a strong adhesion to the substrate. The validity of this hypothesis was confirmed by comparison with further experiments with extra doses at the pattern edge where two more line scans are added than others. The results are shown in Fig. 17. As seen from the equi-energy density contour, a much larger energy is deposited at the edge. This extra dose produces the horn-shaped profile. Although the experimental results show a similar shape to the calculated ones, the position of the horned-shape shifts inside the pattern. This effect is probably caused by the lateral shrinkage above mentioned. The situation of developed resists being stuck at the interface is the same as Fig. 16. Another interesting effect is found in comparison between 1 μm patterns. Namely, the deformation of the experimental profile with the extra dose is smaller than that with the uniform dose. It is because the resist with a larger gel fraction is hard to deform.

Finally, although the problem associated with negative resist requires further study such as the cure effect, the accuracy of the pattern simulation, etc., the present modelling will be helpful for an investigation of the development characteristics of the negative resist such as shrinkage or swelling.

4.3 Time evolution of the developed resist pattern

It is important to know how a developing pattern changes with development time in fabrication processes. This simulation is accomplished by combining the spatial distribution of absorbed energy with the solubility rate as mentioned previously. Theoretical studies on the time evolution for practical application have been published by many authors by calculating the spatial distribution of energy dissipation either by an analytic method or Monte Carlo calculation. Among them Neureuther et al. (1979) made a quantitative comparison between theory and experiment for PMMA resist patterns developed by a solution of MIBK (methyl isobutyl ketone): IPA (isopropyl alcohol) = 1:1. Their experiments of a single line exposure and an array of small lines and spaces was performed by varying the dose slightly at fixed development time rather than varying the development time at constant dose. They simulated the profiles by using both the spatial energy distribution obtained with the Monte Carlo calculation and the solubility rate in which the constants were experimentally obtained separately. Although they obtained a general agreement in profile shape between both results, it was found that there are some discrepancies in that the experimental results show more roundness at the surface edge and a side wall slope than predicted by the theory, and that it is necessary to use a different constant in the solubility rate equation from the constants above mentioned in order to match both results.

Murata et al. (1979) have performed a similar experiment to Neureuther et al. (1979) and compared it with theoretical calculation. The resist thickness, the incident energy and the probe size are 6000 Å, 20 keV and 5500 Å, respectively. The solubility rate constants utilized in the calculation are basically the same as Neureuther, i.e., $R_0 = 0$, $B = 1.0$, $A = 2$. The Monte Carlo simulation was based on the Spencer-Fano theory. Profiles were obtained at several different development times for exposure patterns of a single line and multilines. In Figs. 18 and 19 the comparison is shown for two typical exposure patterns of a single line at a dose of 2.4×10^{-3} C/cm^2 and of six lines spaced by 0.5 μm at a dose of 1.2×10^{-3} C/cm^2. They confirmed a discrepancy similar to that by Neureuther et al. (1979) between both results and found that the solubility rate constant B had to be increased with an increase in dose in order to fit an absolute value of development time to experimental one and it approaches the value B which was obtained from the experiment of a large area exposure.

Later, Rosenfield and Neureuther (1981) attempted to improve the development simulation model by introducing a directional constant in the solubility rate with the string model, which is selected to cause a fast development along the incident electron direction. They found that this effect is more dominant in the single line exposure where there is a smaller contribution of non-directional electrons due to backscattered electrons, compared to multiline exposures.

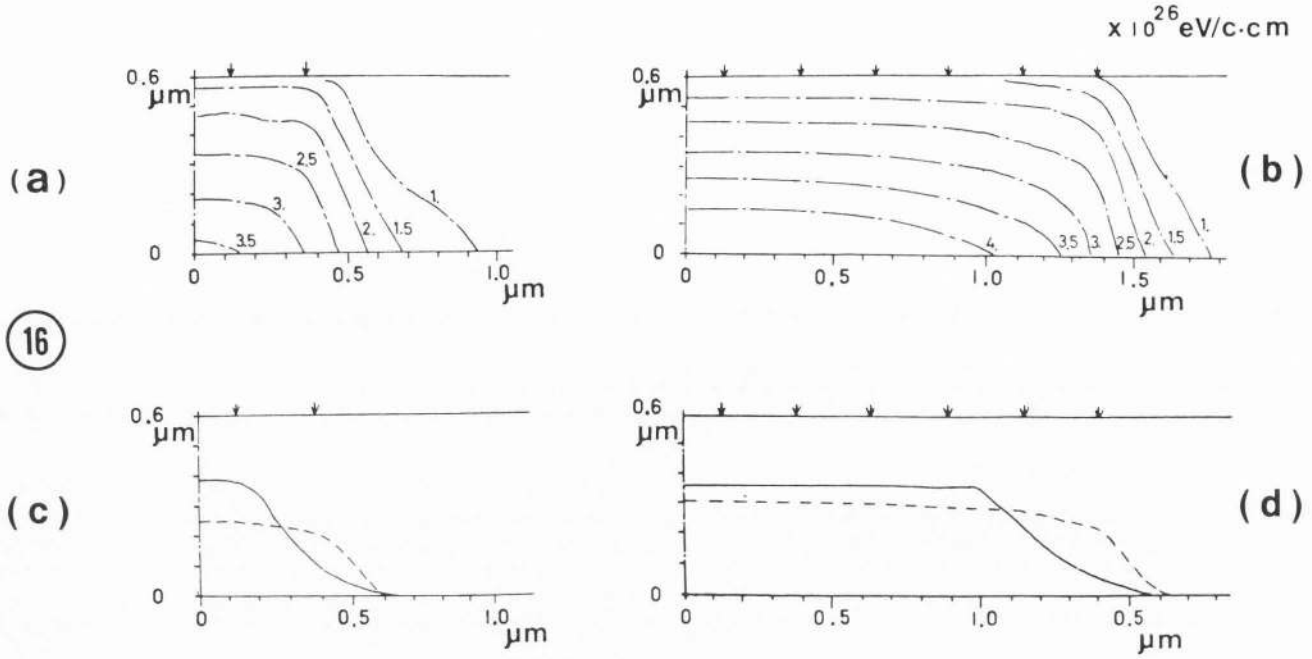

Fig. 16. (a), (b) the equi-energy density contours and (c), (d) developed cross sectional profiles for negative resist patterns of line and spaces. The widths of line and space are (a), (c) 1 μm and (b), (d) 3 μm. The initial beam energy is 10 keV. Solid lines: experiment (Nakata et al. 1981). Dashed lines: Monte Carlo calculation. Profiles are compared at a dose of 4.0×10^{-7} C/cm^2.

Fig. 17. (a), (b) the equi-energy density contours and (c), (d) developed cross sectional profiles for the same patterns as in Fig. 16 except with extra doses at the edges. Solid lines: experiment (Nakata et al. 1981). Dashed lines: Monte Carlo calculation.

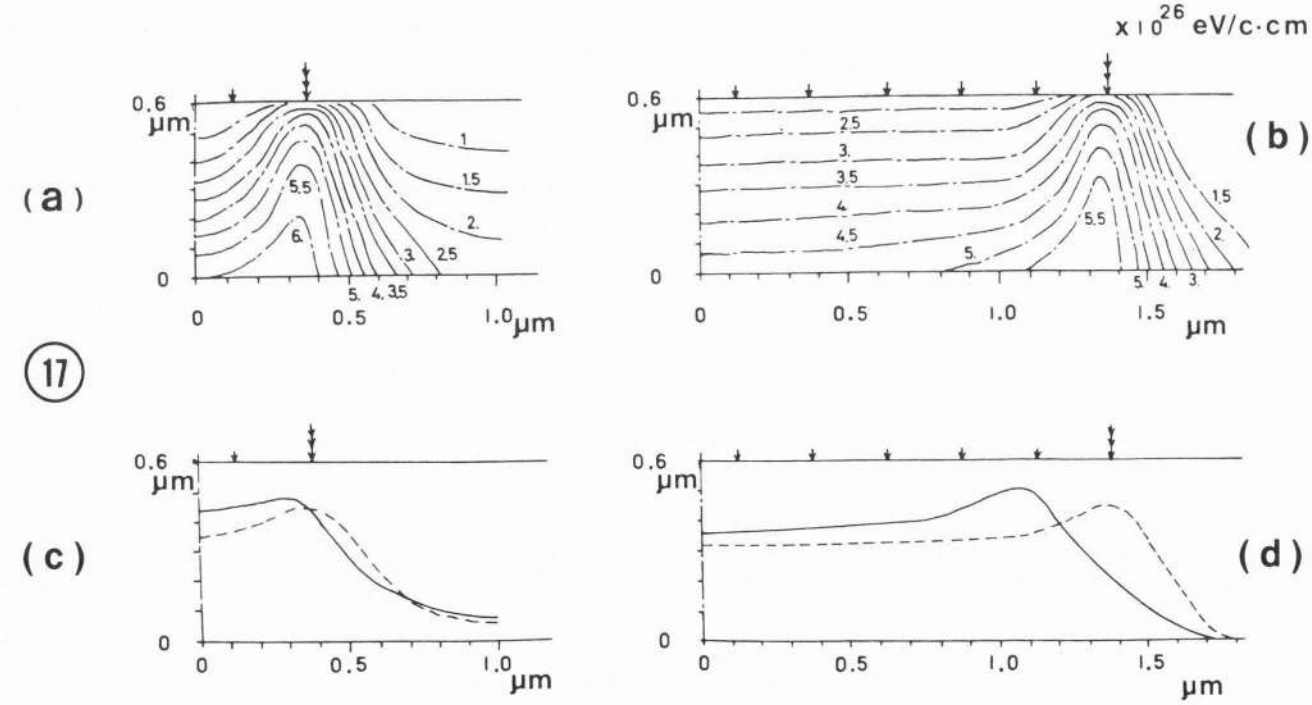

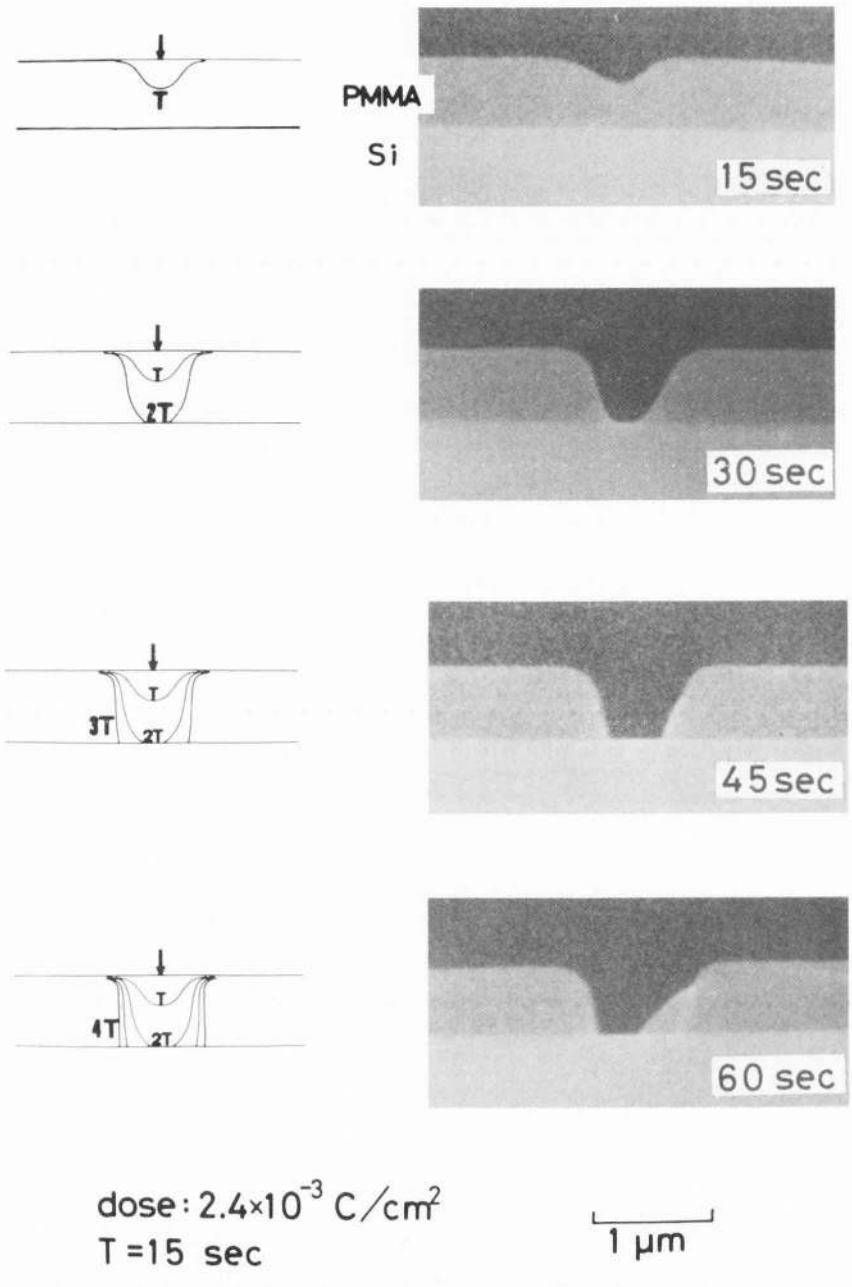

Fig. 18. The time evolution of cross sectional profiles for a single line exposure at a dose of 2.4×10^{-3}C/cm^2. T = 15 sec. B = 0.5 Å/sec.

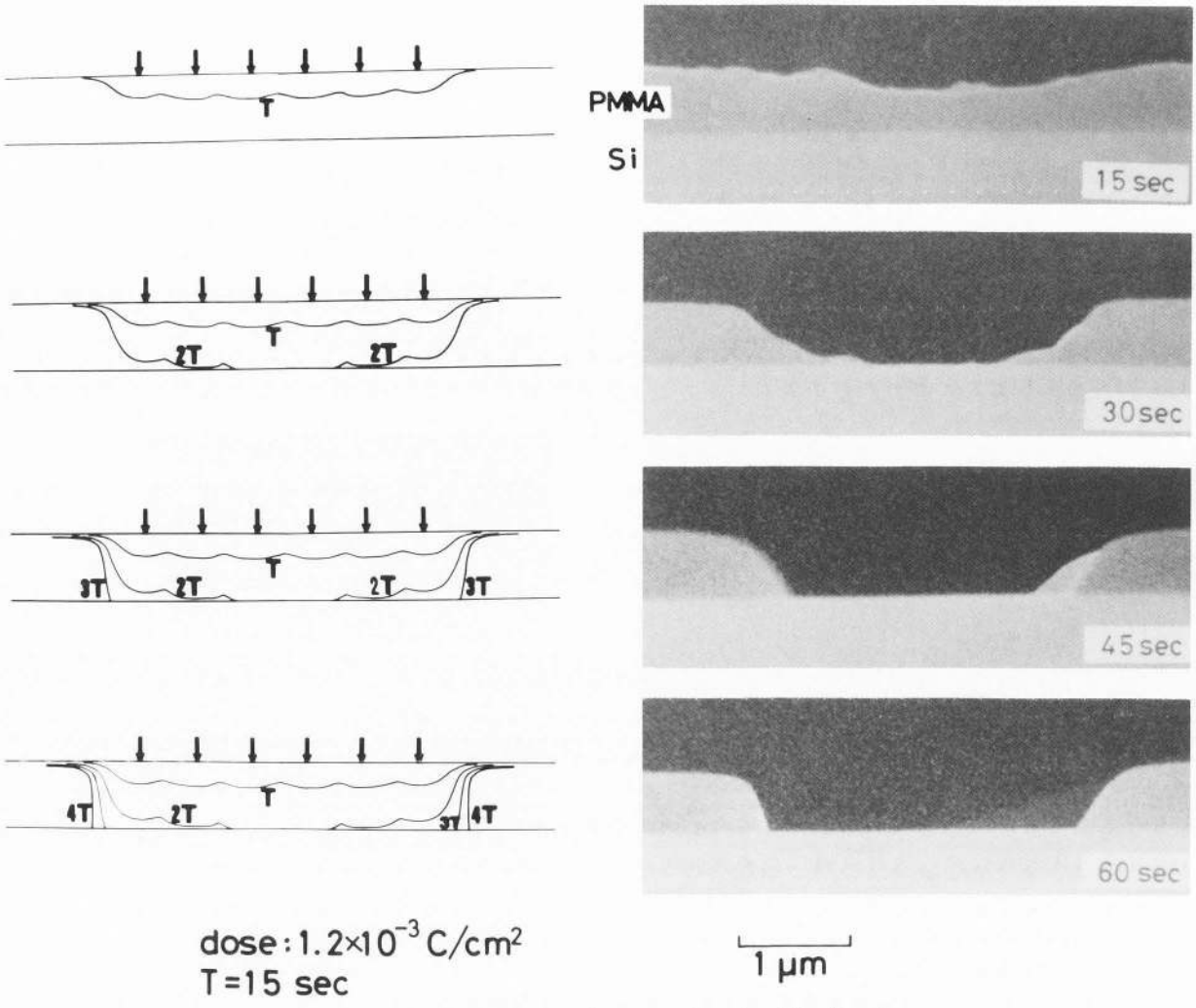

Fig. 19. The time evolution of cross sectional profiles for six line exposures at a dose of 1.2×10^{-3} C/cm². T = 15 sec. B = 0.89 Å/sec.

They suggested that the physical mechanism of the effect is related to the generation of volatile products and micropores in the resist. If it can be assumed that this generation increased with an increase in dose and the solubility rate becomes larger, totally keeping a directional etching, this may explain the use of a larger value of B which was found in the experimental results of Murata et al. (1979). This problem has to be investigated further in more details.

4.4 Resolution limit

The resolution limit for a line exposure was investigated for an isolated thin film of 4000 Å PMMA at 20 keV. Time evolution calculated with the new and the old models is shown in Fig. 20 for a developer of MIBK:IPA = 1:1 at a dose of 50 μC/cm². In the figure clear differences are found in development time and the developed widths between both results. It takes a longer development time to go through the film with the new model because it spreads out the energy dissipation in more wide space. The old model does not show a further development with an increase in time near the surface, while the new one does due to energy absorption by secondary electrons. Let's evaluate the resolution from the developed profile in Fig. 20. According to a previous discussion, the line width is measured in the plane at 1000 Å below the resist surface. The widths were measured from the first profile that goes through the film. These are 530 Å and 320 Å with the new and the old models, respectively. The former value gives a favorable value in comparison with the width of 600 Å obtained experimentally by Sedgwick et al. (1972) at 25 keV with a very thin substrate where the backscattering effect is not significant.

In Fig. 21 the energy distribution, $d\eta/dE$, of fast secondaries generated per one incident electron is shown to see how large energy electrons cause the spatial spreading of the energy absorption in Fig. 20. The largest energy is 10 keV with the initial energy of 20 keV. But there are few secondary

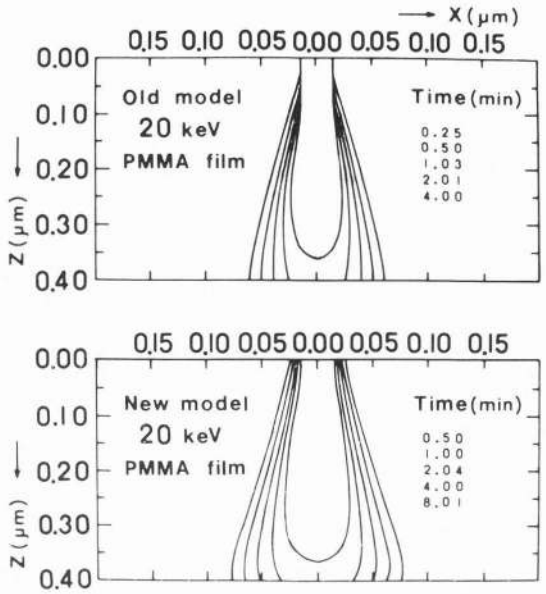

Fig. 20. Calculated developed profiles for an isolated PMMA film of 4000 Å at 20 keV. The probe diameter is 100 Å. Development is made with a 1 to 1 solution of MIBK and IPA. The minimum width is measured at a depth of 1000 Å from the resist surface.

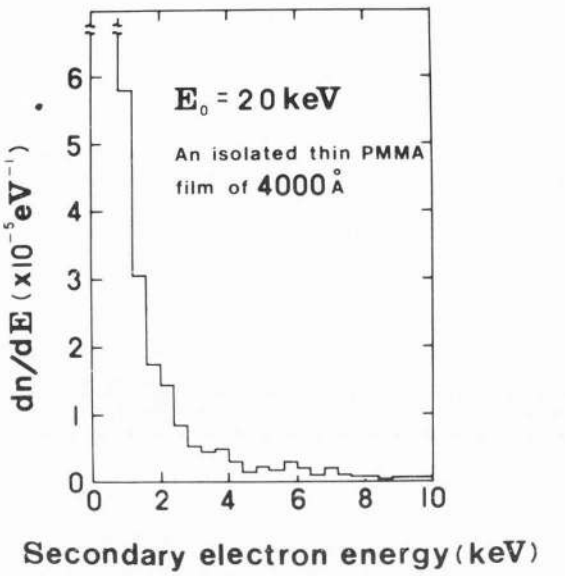

Fig. 21. The energy distribution of fast secondary electrons produced in the same sample as in Fig. 20 through knock-on processes.

electrons with such high energies. The intensity increases rapidly near a few keV energy with decreasing energy. For example let's take the secondary electrons with energies of 1 to 2 keV. These electrons have an ability to deposit about ten to twenty times more energy than a primary electron of 20 keV energy according to a simple estimate with the energy loss law of 1/E and yet are generated at a rate of 573/20000 = 2.8%. Their Bethe ranges are 440 Å to 1400 Å. Therefore these electrons seem to have a significant influence on the ultimate resolution. However, difficulty of the present theory is that the accuracy of the Bethe law at low energies and the cross section for fast secondary electron production are not sufficiently clear at the present.

ACKNOWLEDGMENT

The author would like to express his thanks to Prof. K. Nagami (University of Osaka Prefecture) for his constant encouragement. He owes Dr. D. Kyser (Philips research laboratory, Signetics) for his contribution to simulation modelling of fast secondary electron production and revision of the manuscript. He also would like to thank Dr. M. Kotera and Mr. K. Nozaki for their assistance in preparing the manuscript.

REFERENCES

Adesida I and Everhart TE. (1980). Limitations due to electron scattering in electron beam lithography. Proc. 9th Int. Conf. on Electron and Ion Beam Sci. Technol., R. Bakish (ed.), Electrochem. Soc., Pennington, NJ, p. 189-199.

Adesida I, Everhart TE and Shimizu R. (1979). High resolution electron-beam lithography on thin films. J. Vac. Sci. Technol. **16**, 1743-1748.

Atoda N and Kawakatsu H. (1976). Gel formation in negative electron resists. J. Electrochem. Soc. **123**, 1519-1524.

Berger MJ. (1963). Monte Carlo calculation of the penetration and diffusion of fast charged particles. Methods in Computational Physics, Vol. 1, B. Alder, S. Fernback and M. Rotenberg (eds.), Academic Press, New York, p. 135-215.

Berger MJ. (1971). Energy deposition by low-energy electrons: delta-ray effects in track structure, and microdosimetric event-size spectra. Proc. of the 3rd Symp. on Microdosimetry, H.G. Ebert (ed.), Euratum Publ., Brussels, p. 157-174.

Berger MJ and Seltzer SM. (1964). Studies in penetration of charged particles in matter. Natl. Acad. Sci.-Natl. Res. Council, Publ. 1133 (Washington, DC), p. 205-268.

Bishop HE. (1966). Calculation of electron penetration and X-ray production. X-ray Optics and Microanalysis, R. Castaing, P. Descamps and J. Philibert (eds.), Hermann, Paris, p. 153-158.

Broers AN. (1981). Resolution limits of PMMA resist for exposure with 50kV electrons. J. Electrochem. Soc. **128**, 166-170.

Brown DB, Wittry DB and Kyser DF. (1969). Prediction of X-ray production and electron scattering in electron-probe analysis using a transport equation. J. Appl. Phys. **40**, 1627-1636.

Chang THP. (1975). Proximity effect in electron-beam lithography. J. Vac. Sci. Technol. **12**, 1271-1275.

Charlesby A. (1954). Gel formation and molecular weight distribution in long-chain polymers. Proc. Roy. Soc., London, **A-222**, 542-557.

Curgenven L and Duncumb P. (1971). Simulation of electron trajectories in a solid target by a simple Monte Carlo technique. Tube Investments Research Report N. 303 (Saffron Walden, Essex, England).

Green M. (1963). A Monte Carlo calculation of the spatial distribution of characteristic X-ray production in a solid target. Proc. Phys. Soc. **82**, 204-215.

Greeneich JS. (1974). Solubility rate of poly- (methyl methacrylate), PMMA, electron resist. J. Electrochem. Soc. **121**, 1669-1671.

Greeneich JS. (1975). Developer characteristics of poly-(methyl methacrylate) electron resist. J. Electrochem. Soc. **122**, 970-976.

Greeneich JS and Van Duzer T. (1974). An exposure model for electron sensitive resists. IEEE Trans. Electron Devices ED-21, 286-299.

Hawryluk RJ. (1981). Exposure and development models used in electron beam lithography. J. Vac. Sci. Technol. **19**, 1-17.

Hawryluk RJ, Hawryluk AM and Smith HI. (1974). Energy dissipation in a thin polymer film by electron beam scattering. J. Appl. Phys. **45**, 2551-2566.

Hawryluk RJ, Smith HI, Soares A and Hawryluk AM. (1975). Energy dissipation in a thin polymer film by electron scattering: experiment. J. Appl Phys. **46**, 2528-2537.

Heidenreich RD, Ballantyne JD and Thompson LF. (1975). Electron scattering and line profiles in negative electron resists. J. Vac. Sci. Technol. **12**, 1284-1288.

Herzog RF, Greeneich JS, Everhart TE and Van Duzer T. (1972). Computer-controlled resist exposures in the scanning electron microscope. IEEE Trans. Electron Devices, ED-19, 635-641.

Horiguchi SM, Suzuki M, Kobayashi T, Yoshino H and Sakakibara Y. (1981). New method of electron free path in multiple layers for Monte Carlo simulation. App. Phys. Lett. **39**, 512-514.

Jewett RE, Hagouel PI, Neureuther AR and Van Duzer T. (1977). Line-profile resist development simulation techniques. Polymer Eng. Sci. **17**, 381-384.

Jones F and Paraszezak J. (1981). RD3D computer simulation of resist development in three dimensions. IEEE Trans. Electron Devices, ED-28, 1544-1552.

Ku HY and Scala LC. (1969). Polymeric electron-beam resists. J. Electrochem. Soc. **116**, 980-985.

Kulchitsky LA and Latyshev GD. (1942). The multiple scattering of fast electrons. Phys. Rev. **61**, 254-265.

Kyser DF and Murata K. (1974). Monte Carlo simulation of electron beam scattering and energy loss in thin films on thick substrates. Proc. 6th Int. Conf. on Electron and Ion Beam Science and Technology, R. Bakish (ed.), Electrochem. Soc., Princeton, NJ, p. 205-223.

Kyser DF and Murata K. (1974). Quantitative electron microprobe analysis of thin films on substrates. IBM J. Res. Develop. **18**, 352-363.

Kyser DF, Schreiber DE and Ting CH. (1980). Proximity function approximations for electron beam lithography from resist profile simulation. Proc. 9th Int. Conf. on Electron and Ion Beam Science and Technology. R. Bakish (ed.), Electrochem. Soc., Pennington, NJ, p. 255-271.

Lin LH. (1975). Cross-section profiles of single scan negative electron-resist lines. J. Vac. Sci. Technol. **12**, 1289-1293.

Love G, Cox MCG and Scott VO. (1977). A simple Monte Carlo method for simulating electron-solid interactions and its application to electron probe microanalysis. J. Phys. **D 10**, 7-23.

McDonald IR, Lamki AM and Delaney CFG. (1971). The attenuation and backscattering of electron beams by thin films. J. Phys. **D 4**, 1210-1217.

Miyatake O and Nakayama T. (1963). Monte Carlo methods, in Japanese (Nikkan Kogyo Shinbun, Tokyo), p. 139-140.

Murata K, Matsukawa T and Shimizu R. (1971). Monte Carlo calculations on electron scattering in a solid target. Jpn. J. Appl. Phys. **10**, 678-686.

Murata K, Nomura E, Nagami K, Kato T and Nakata H. (1979). Experimental and theoretical study of cross-sectional profiles of resist patterns in electron-beam lithography. J. Vac. Sci. Technol. **13**, 1734-1738.

Murata K, Kotera M and Nagami K. (1980). Surface distribution of backscattered electrons in the SEM and EPMA. Proc. 8th Int. Conf. on X-ray optics and Microanalysis, O.R. Beaman, R.E. Ogilvie and D.B. Wittry (eds.), Pendell Publ. Corp., Michigan, p. 434-438.

Murata K, Kyser DF and Ting CH. (1981). Monte Carlo simulation of fast secondary electron production in electron beam resists. J. Appl. Phys. **52**, 4396-4405.

Nakata H, Kato T, Murata K, Hirai Y and Nagami K. (1981). The effect of extra doses at the pattern edges on negative electron resist profiles. J. Vac. Sci. Technol. **19**, 1248-1253.

Neureuther AR, Kyser DF and Ting CH. (1979). Electron-beam resist edge profile simulation. IEEE Trans. Electron Devices ED-26, 686-693.

Newbury DE, Myklebust RL and Heinrich KFJ. (1980). A hybrid Monte Carlo procedure employing single and multiple scattering. Proc. 8th Int. Conf. on X-ray Optics and Microanalysis, O.R. Beaman, R.E. Ogilvie and D.B. Wittry (eds.), (Pendell Publ. Corp., Michigan), p. 57-62.

Nigam BD, Sundaresan MK and Wu T-Y. (1959). Theory of multiple scattering: second Born approximation and corrections to Moliere's work. Phys. Rev.**115**, 491-502.

Rao Sahib T and Wittry DB. (1974). X-ray continuum from thick elemental targets for 10-50 keV electrons. J. Appl. Phys. **45**, 5060-5068.

Reimer L. (1968). Monte-Carlo-rechnungen zur elektronendiffusion. (Monte Carlo calculation of electron diffusion.) Optik, **27**, 86-98.

Reimer L, Gilde H and Sommer KH. (1970). Die verbreiterung eines elektronen strahles (17-1200keV) durch mehrfachstreuung. (The broadening of an electron beam (17-1200 keV) by multiple scattering.) Optik, **30**, 590-605.

Rosenfield MG and Neureuther AR. (1981). Exploration of electron-beam writing strategies and resist development effects. IEEE Trans. Electron Devices, ED-28, 1289-1294.

Saito N. (1973). Monte Carlo simulation for the energy dissipation profiles of 5-20 keV electrons in layered structures. Jpn. J. Appl. Phys. **12**, 941-942.

Schneider DO and Cormack DV. (1959). Monte Carlo calculations of electron energy loss. Radiation Research, **11**, 418-429.

Sedgwick TO, Broers AN and Agule BJ. (1972). A novel method for fabrication of ultrafine metal lines by electron beams. J. Electrochem. Soc. **119**, 1769-1771.

Seltzer SM. (1974). Transmission of electrons through foils. Natl. Bur. Stand. Rept. NBSIR 74-457 (Washington, D.C.)

Shimizu R. (1974). Secondary electron yield with primary electron beam of kilo-electron-volts. J. Appl. Phys. **45**, 2107-2111.

Shimizu R, Murata K and Shinoda G. (1966). Depth distribution of characteristic X-ray in microanalyser target. X-ray Optics and Microanalysis, R. Castaing, P. Descamps and J. Philibert (eds.), Hermann, Paris, p. 127-138.

Shimizu R and Everhart TE. (1972). Monte Carlo simulation of the energy dissipation of an electron beam in an organic specimen. Optik, **36**, 59-65.

Shimizu R, Ikuta T, Everhart TE and DeVore WJ. (1975). Experimental and theoretical study of energy dissipation profiles of keV electrons in polymethyl methacrylate. J. Appl. Phys. **46**, 1581-1584.

Shimizu R, Kataoka Y, Ikuta T, Koshikawa T and Hashimoto H. (1976). A Monte Carlo approach to the direct simulation of electron penetration in solids. J. Phys. **D 9**, 101-114.

Shinoda G, Murata K and Shimizu R. (1968). Scattering of electrons in metallic targets. Quantitative Electron Probe Microanalysis, K.F.J. Heinrich (ed.), Nat. Bur. Stand., Special Publ. 298, Washington, D.C., p. 155-187.

Spencer LV and Fano U. (1954). Energy spectrum resulting from electron slowing down. Phys. Rev. **93**, 1172-1187.

Wolf EO, Ozdemir FS, Perkins WE and Coane PJ. (1971). Response of the positive electron resist elvacite 2041 to kilovolt electron beam exposure. Rec. of 11th Symp. on Electron, Ion and Laser Beam Technology, R.F.M. Thornley (ed.), San Francisco Press, San Francisco, p. 331-336.